Assessing morphological changes in a human-impacted fluvial system by hydro-sediment modeling and remote sensing

Mohammad Reza Shojaeian[a], Zahra Karimidastenaei[a*], Omid Rahmati[b], Ali Torabi Haghighi[a]

[a]Water, Energy and Environmental Engineering Research unit, University of Oulu, P.O. Box 4300, FIN-90014 Oulu, Finland.
[b]Soil Conservation and Watershed Management Research Department, Kurdistan Agricultural and Natural Resources Research and Education Center, AREEO, Sanandaj 6616936311, Iran.
*Corresponding author: Email: zahra.karimidastenaei@oulu.fi

Abstract

Construction of managed aquifer recharge structures (MARS) to store floodwaters is a common strategy for recovering depleted groundwater resources in arid and semi-arid regions, as part of integrated water resources management (IWRM). MARS diverts surface water to groundwater, but this can affect downstream fluvial processes. The impact of MARS on fluvial processes was investigated in this study by combining remote sensing techniques with hydro-sediment modeling for the case of the Kaboutar-Ali-Chay aquifer, Northwestern Iran. We assessed the impact of MARS on groundwater dynamics, modeled sedimentation across the MARS using a 2D hydrodynamic model, and quantified morphological changes in the human-impacted alluvial fan using Landsat time series data and statistical methods. Changes were detected by comparing data for the periods before (1985-1996) and after (1997-2018) MARS construction. The results showed that the rate of groundwater depletion decreased from 2.14 m/year before to 0.86 m/year after MARS construction. Hydro-sediment modeling revealed that MARS ponds slowed water outflow, accompanied by a severe decrease in sediment load, leading to a change from sediment deposition to sediment erosion in the alluvial fan. Morphometric analyses revealed decreasing alluvial fan area and demonstrated significant differences ($p<0.01$) between pre- and post-impact periods for different morphometric parameters analyzed. The rate of change in area of the

Kaboutar-Ali-Chay alluvial fan changed from -0.228 to -0.115 km^2/year between pre- and post-impact periods.

Keywords: Groundwater Recharge; MARS; CCHE2D; Landsat; Statistical analysis.

1. Introduction

Water resources are an essential foundation for social development world-wide (Yang et al., 2019; Chang et al., 2020). Access to fresh, clean water is critical for the sustainability of human society and is strongly influenced by heterogeneities in the spatio-temporal distribution of water resources (Liu et al., 2019). The world is now facing enormous challenges in supplying water to support the increasing urbanization, industrialization, and agricultural development required by rapid population growth (Ohlsson, 2000). Therefore, many efforts are being made to overcome water shortages and inadequate water resources, particularly in arid and semi-arid regions (Abou Zaki et al., 2019; Torabi Haghighi et al., 2020a). However, these efforts can lead to unsustainable use of water resources and can have many socio-economic and environmental impacts (Torabi Haghighi et al., 2014; Pirnia et al., 2019; Fazel et al., 2017).

Surface water resources are scarce in arid and semi-arid regions and increasing demand for surface water reserves, in combination with increasing pollution of rivers, lakes and other sources of water, is creating a crisis of supply (Torabi Haghighi et al., 2018). Therefore, groundwater resources are being exploited as an alternative to fresh surface water to overcome droughts and water shortages (Torabi Haghighi et al., 2020b). In arid and semi-arid areas, overexploitation of groundwater resources can lead to declining groundwater levels, so water conservation measures such as managed aquifer recharge structures (MARS) at regional and local scale are of great importance (Zaki et al., 2018; Yaraghi et al., 2019). Within integrated water resources management (IWRM), MARS are an appropriate strategy for flood control, groundwater recharge, and provisioning a stable fresh water supply to meet domestic and agricultural demand (Lin and Wei, 2006; Liu et al., 2010; Huang et al., 2013; Tan et al., 2017). However, MARS, which mainly involves damping flood flows in constructed ponds, can affect landscape and environment, e.g., geomorphological features such as river morphology (Beigi and Tsai, 2015; Han et al., 2017; Huang et al., 2019; Shahrood et al., 2020).

The impact of hydraulic structures, e.g., dams and MARS, on river flow regime, geomorphology, and environments is well-documented, but the impact of MARS on other natural features, e.g., alluvial fans, has been less well studied. In general, MARS and other hydraulic structures significantly alter sediment dynamics, e.g., damping the flood regime in ponds results in the majority of sediment being trapped in the ponds (Poeppl et al., 2017). This leads to reduced sediment transport and changes in natural features downstream. Sediment transport (erosion/deposition) is a major process in the formation of alluvial fans, and MARS could significantly affect this process as an unwanted side-effect of water resources management (Giardino et al., 2007; Volpe et al., 2011).

Assessing sedimentation in MARSs is important, as sediment build-up decreases the efficiency of groundwater recharge by reducing bed permeability and reduces the amount of sediment transported to downstream alluvial features. The motivation behind the monitoring morphological changes in a human-impacted fluvial system and assessing sedimentation in MARSs, which is interesting in fruitful as interdisciplinarity and multidisciplinary of sciences (water resources management and river engineers fields) inspired us to combine the hydro-sediment dynamic modeling procedures, remote sensing techniques and statistical methods. Therefore, the main aims of this study were to: *i*) assess the hydrological impacts of MARSs on groundwater levels, *ii*) determine the impact of MARS on erosion/deposition process, using hydro-sediment dynamic modeling, and *iii*) monitor and quantify morphological changes in the downstream alluvial fan using remote sensing techniques and statistical methods. The novelty of this study contributes to all above mentioned goals including new effective methodology, techniques and data which leads to new knowledge and information discovery on sedimentation in MARSs, groundwater level and morphological changes of alluvial fan simultaneously. The Kaboutar-Ali-Chay alluvial fan in Iran was used as a case.

2. Materials and methods

2.1. Study area

The Kaboutar-Ali-Chay alluvial fan (38°08′45″-38°13′15″N; 45°34′20″-45°37′39″E) is located on the Shabestar plain in Azarbaijan-e Sharqi province, Northwestern Iran (Fig. 1). It has a general north-south slope and falls within Lake Urmia basin. The cities of Khameneh, Kuzah-kenan, and Shandabad are the main population centers located on the Kaboutar-Ali-Chay alluvial fan. According to metrological data from Shabestar station (1985-2018), mean annual precipitation in the region is 320 mm, maximum temperature is 28°C (in July) and minimum temperature is -18°C (in January). The MARS for Kaboutar-Ali-Chay, constructed in 1996, comprises seven ponds located at the top of the alluvial fan (Fig. 1). The diverted floodwater flow to the ponds leads to artificial aquifer recharge by raising the groundwater level. The main formation of the Shabestar plain comprises young Quaternary and alluvial sediments (Qf2, Qt3), while some parts of the Kaboutar-Ali-Chay alluvial fan consist of clay zones.

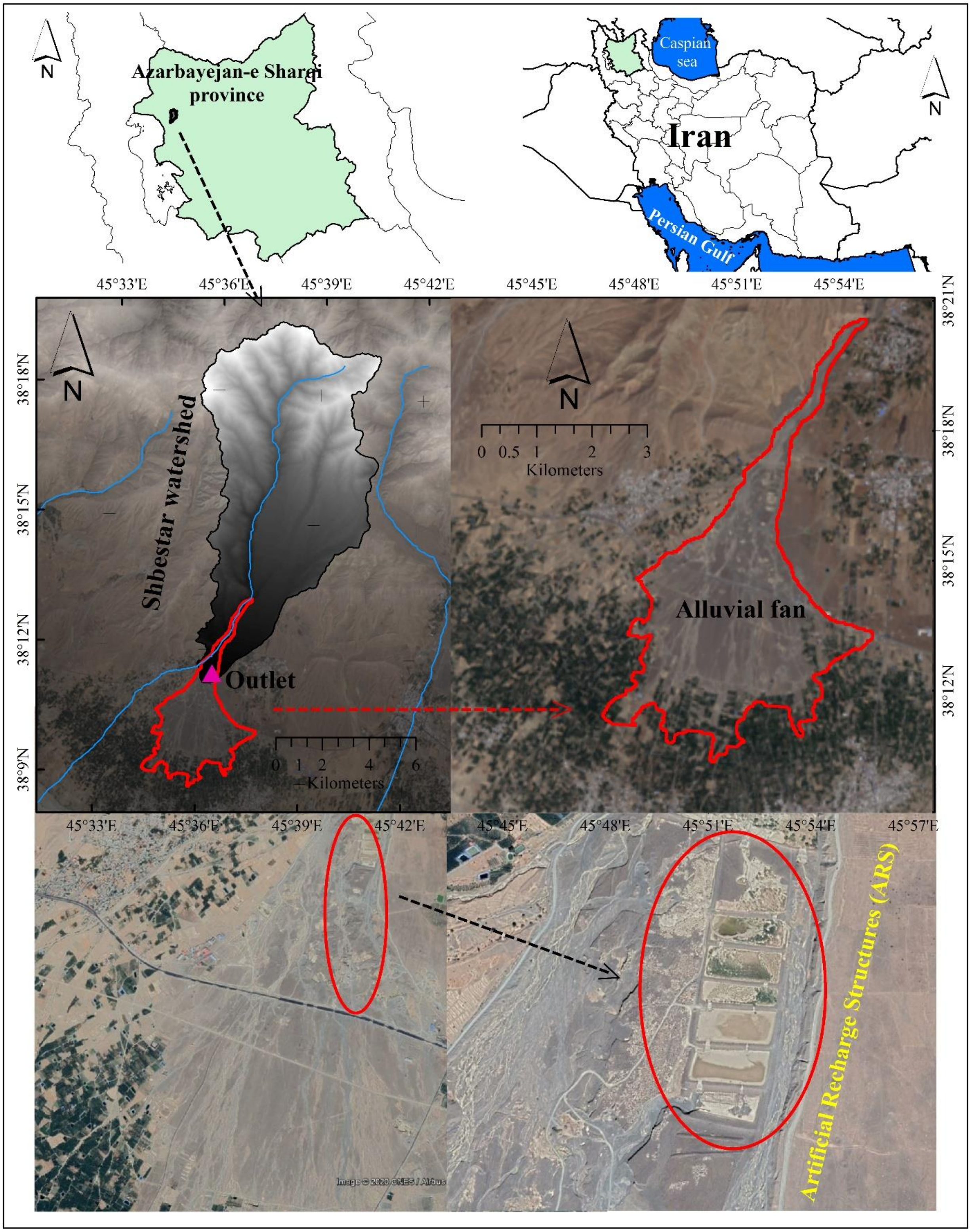

Fig. 1. Maps showing location of the study area in Azarbaijan-e Sharqi province, Northwestern Iran, and of artificial aquifer recharge structures on the alluvial fan at the outlet of Shibestar watershed.

2.2 Methodology

The present work consisted of three steps: 1) Groundwater dynamics were analyzed to assess the performance of MARS in the Kaboutar-Ali-Chay aquifer. 2) Hydro-sediment modeling of MARS ponds was carried out using 2D hydrodynamic CCHE2D model, to determine the deposition process. 3) Morphological changes in the alluvial fan were assessed using remote sensing data (Landsat images) and statistical analysis.

2.2.1 Groundwater level analysis

Times series of data from groundwater observation wells downstream of Kaboutar-Ali-Chay MARS (see Fig. 1) were analyzed to assess the role of the structure on groundwater levels in the aquifer (Kalbus et al., 2006; Lu et al., 2014; Cai and Ofterdinger, 2016). Mann-Kendall and Sen's slope estimator, two nonparametric statistical methods widely used for hydro-climatological purposes (Sang et al., 2014; Lu et al., 2015; Bari et al., 2016; Haghighi et al., 2020), were applied in analysis of observed precipitation and groundwater level trends in pre- and post-MARS construction periods.

2.2.2 Hydro-sediment modeling in managed aquifer recharge structures (MARS)

Hydro-sediment modeling was performed using the hydrodynamic Center for Computational Hydro-science and Engineering 2 Dimension (CCHE2D) model developed at the National Center for Computational Hydro-science and Engineering (NCCHE), University of Mississippi. It has been demonstrated to have good capabilities in the field of water and sediment simulation. The latest version, CCHE2D 3.2 (Kamanbedast et al., 2018), was used in this study to simulate flow and sediment transport at the Kaboutar-Ali-Chay MARS. In CCHE2D (Jia and Wang, 1999; Zhang and Jia, 2005; Zhang and Jia, 2013), continuity (Eq.1) and momentum equations (Eqs. 2 and 3) are used to solve the depth-integrated two-dimensional Navier-Stokes equation (Eq. 1-4):

$$\frac{\partial Z}{\partial t}+\frac{\partial(hu)}{\partial x}+\frac{\partial(hv)}{\partial y}=0 \tag{1}$$

$$\frac{\partial u}{\partial t}+u\frac{\partial u}{\partial x}+v\frac{\partial u}{\partial y}=-g\frac{\partial Z}{\partial x}+\frac{1}{h}\left[\frac{\partial(h\tau_{xx})}{\partial x}+\frac{\partial\left(\left(h\tau_{xy}\right)\right)}{\partial y}\right]+\frac{\tau_{wx}-\tau_{tx}}{\rho h}+f_{cor}v \tag{2}$$

$$\frac{\partial u}{\partial t}+u\frac{\partial u}{\partial x}+v\frac{\partial u}{\partial y}=-g\frac{\partial Z}{\partial x}+\frac{1}{h}\left[\frac{\partial(h\tau_{xx})}{\partial x}+\frac{\partial\left(\left(h\tau_{xy}\right)\right)}{\partial y}\right]+\frac{\tau_{wx}-\tau_{tx}}{\rho h}-f_{cor}v \tag{3}$$

$$\left(\tau_{wx},\tau_{wy}\right)=\rho_{air}c_{fa}\sqrt{U_w^2+V_w^2}+(U_w,V_w) \tag{4}$$

where u and υ are components of the depth-integrated velocity in the x and y directions, respectively, g is gravitational force, Z is elevation of the water surface, ρ is water density, h is local water depth, f_{Cor} is the Coriolis parameter, τ_{bx}, τ_{by} and τ_{wx}, τ_{wy} are shear stresses on the bed and surface water, respectively, C_{fa} is friction coefficient at the water surface, U_w and V_w are velocity of water, and τ_{xx}, τ_{xy}, τ_{yx}, and τ_{yy} are stresses at depth, integrating both viscous and turbulent effects, approximated based on Boussinesq's assumption:

$$\tau_{xx}=2\rho(v+v_t)\frac{\partial u}{\partial x} \tag{5}$$

$$\tau_{xx}=\tau_{yx}=\rho(v+v_t)(\frac{\partial u}{\partial y}+\frac{\partial v}{\partial x}) \tag{6}$$

$$\tau_{yy}=2\rho(v_t+v)\frac{\partial v}{\partial y} \tag{7}$$

where υ is the kinematic water viscosity. Two zero-equation eddy viscosity models, namely the parabolic model and the mixing length model, and the more sophisticated two-equation k–e turbulence model is used in the CCHE2D model to calculate eddy viscosity υ_t (Nassar, 2011; Zhang and Jia, 2013).

Required data for CCHE2D are digital elevation model (DEM), discharge and sediment data, and data on particle size distribution in beds and on suspended load particle size. The latter were obtained from Azarbaijan-e Sharqi Regional Water Company in the present case.

2.2.3 Procedure of the CCHE2D

The CCHE2D model was applied to simulate flow and sediment transport in the Kaboutar-Ali-Chay MARS. The modeling procedure involved using ArcGIS to make a DEM with topographic data, a mesh generator, and a Graphical User Interface (GUI) to govern equations (continuous and momentum) in CCHE2D for simulating flow. Schematic diagrams of MARSs is presented in the Fig. 2.

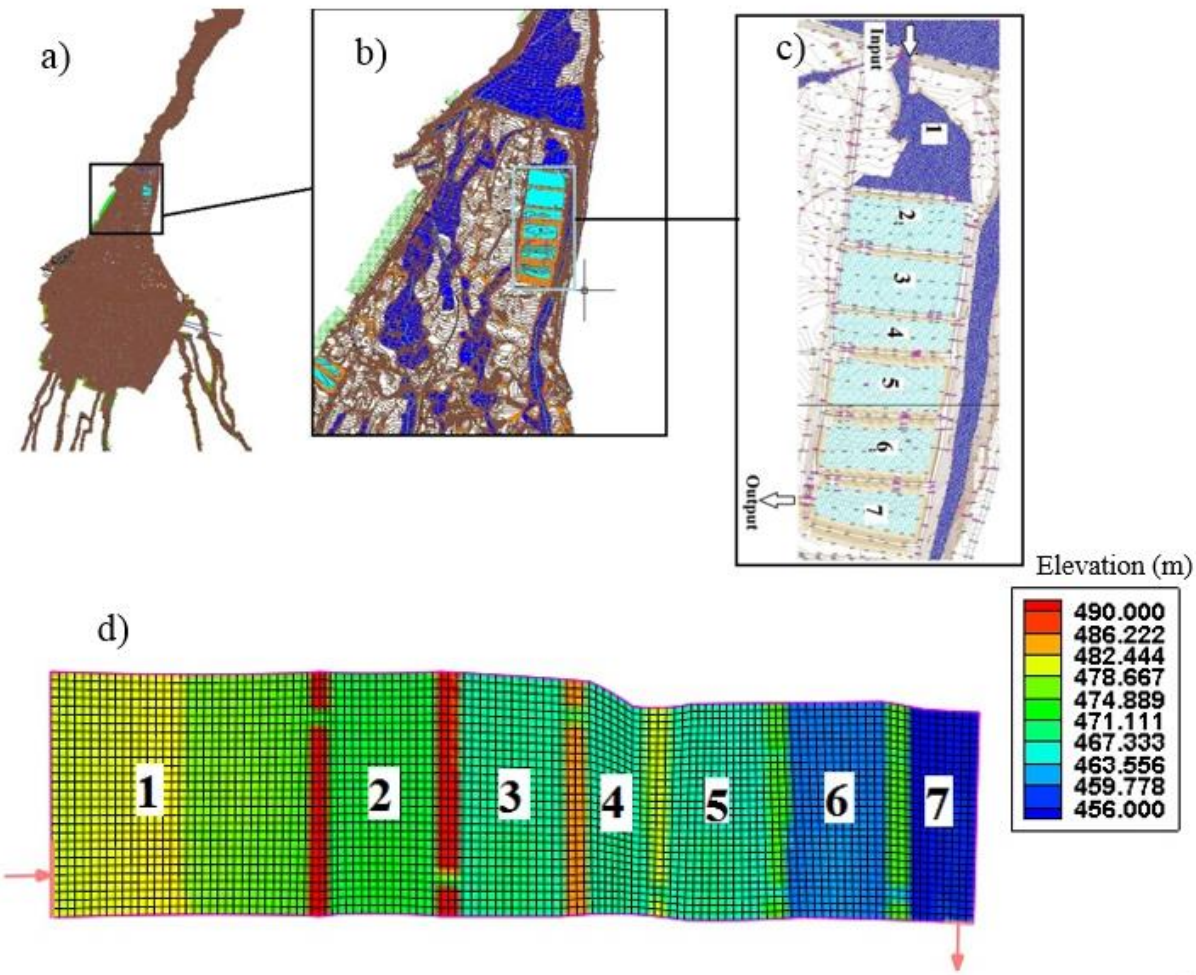

Fig. 2. Schematic diagrams of managed artificial recharge structures (MARS). a) Kaboutar-Ali-Chay alluvial fan; b, c) MARS ponds 1-7, and d) mesh and boundary conditions for MARS components.

After entering the geometric data on MARS into the CCHE2D model and determining the boundaries of the studied reach (size of ponds), a numerical mesh was generated using orthogonal mesh. The orthogonality of the mesh was evaluated using two indices, averaged deviation from orthogonality (ADO) and maximum deviation from orthogonality (MDO). The smoothness of the mesh structure was evaluated based on two other indices, averaged grid aspect ratio (AGAR) and maximum grid aspect ratio (MGAR) (Moussa, 2010; Rad et al., 2019). High quality of the mesh structure was assumed at lower values for the orthogonality indices and values closer to 1 for the smoothness indices, (Zhang and Jia, 2013). The equations for the indices are:

$$MDO = \max(\theta_{i,j}) \tag{8}$$

$$ADO = \frac{1}{n_{i-2}}\frac{1}{n_{j-2}}\sum_{2}^{n_{i-1}}\sum_{2}^{n_{j-1}}\max(\theta_{i,j}) \tag{9}$$

$$\theta_{i,j} = arcCos(\frac{g12}{h_{\xi}h_{\eta}})_{i,j} \tag{10}$$

$$\text{MGAR} = \max\left[max\left(f_{i,j,}\frac{1}{f_{i,j}}\right)\right] \tag{11}$$

$$AGAR = \frac{1}{n_{i-2}}\frac{1}{n_{j-2}}\sum_{2}^{n_{i-1}}\sum_{2}^{n_{j-1}}\max\left[max\left(f_{i,j,}\frac{1}{f_{i,j}}\right)\right] \tag{12}$$

where MDO, ADO are orthogonality indices, MGAR and AGAR are smoothness indices, n_i and n_j are maximum and minimum of the mesh in direction ξ and η, respectively, ξ and η are coordinates in direction x and y, respectively, and g_{12} is a metric tensor.

2.2.3. Quantifying morphological change in the alluvial fan

The rate of change in the Kaboutar-Ali-Chay alluvial fan was determined by quantifying morphometric variations using a time series of Landsat satellite images (1984-2017). This is a novel application of Landsat images and demonstrates their utility in improving understanding of the complex spatial and temporal dynamics of fluvial systems. The Landsat images used consisted of Landsat 5-Thematic Mapper (TM), Landsat 7-Enhancement Thematic Mapper plus (ETM+), and Landsat 8-Operational Land Imager (OLI) multispectral images acquired in 1984, 1987, 1990, 1993, 1996, 1999. 2002, 2005, 2008, 2011, 2014 and 2017 (http://glovis.usgs.gov. The TM, ETM+ and OLI images were obtained in the form of raw digital data, requiring radiometric calibration and atmospheric correction of the images to generate consistent, high-quality image materials (Chander, Markham, & Helder, 2009; Yang et al., 2015). For radiometric calibration of the images we used TOA reflectance, based on advantages reported by Li et al. (2013). We then performed atmospheric correction on the TOA reflectance data for all images using the FLAASH (Fast Line-of-Sight Atmospheric Analysis of Spectral Hypercubes) module in ENVI 5.3. After pre-processing of the Landsat data, a map of the alluvial fan was extracted using the supervised classification and maximum likelihood algorithm in ENVI 5.3. Finally, in morphometric analysis seven indices were employed to classify images in Arc GIS 10.5 (Table 1): Length of alluvial fan (L_{AF}), form factor (R_f), shape factor (S_{AF}), elongation ratio (R_e), circularity ratio (R_c), compactness coefficient (C_c), and slope (S). Full descriptions of all morphometric parameters can be found in Sindhu et al. (2015), Arab Ameri et al. (2018), and Poongodi and Venkateswaran (2018).

Table 1. Morphometric characteristics of the Kaboutar-Ali-Chay alluvial fan

Morphometric parameter	Formula	Units
Length of alluvial fan	$L_{AF} = 1.312A^{0.568}$	km
Form factor	$R_f = A/L_{AF}^2$	–

Shape	$S_{AF} = L_{AF}^2/A$	–
Elongation ratio	$R_e = 1.128A^{0.5}/L_{AF}$	–
Circularity ratio	$R_c = 12.57A/P^2$	–
Compactness coefficient	$C_c = 0.2821P/A^{0.5}$	–
Slope	(x2-x1/y2-y1) * 100	%

2.2.6. Statistical analysis of morphological parameters

Application of the Kolmogorov-Smirnov test (Koller et al., 2013; Haghighi et al., 2019) revealed that the time series of data on morphological parameters were normally distributed ($p>0.05$). Therefore, differences in the seven morphological parameters before and after MARS construction were assessed using paired samples t-test (Hartmann et al., 2016; Sohn et al., 2020). All statistical analyses were carried out using SPSS 23.v software.

3. Results and discussion

3.1. Performance of MARS

The performance of MARS was assessed by analysis of temporal variations in precipitation and groundwater levels 1985-2018 (Fig. 3). No significant trend was observed in precipitation value, but there was a positive tendency in the amount of precipitation (positive value for Mann-Kendall test and Sen's slope) during 1985-2018 (Fig. 3 and Table 2). In the same period, the groundwater level in the Shabestar aquifer showed a significant negative trend, declining by approximately 25 m by 2018, despite the positive trend in precipitation value (Fig. 3 and Table 2). This decline reflected the significant influence of anthropogenic activities (e.g., irrigation, domestic, and industrial water usages) on available water resources in the area. The dramatic decline in groundwater level led to the construction of the Kaboutar-Ali-Chay MARS in 1996 to recharge groundwater resources. Although the groundwater level did not recover entirely or even stabilize by 2018 due to MARS construction, the rate of decline in the groundwater level gradually became smaller (Fig. 3). In the period before MARS construction (1985-1996), the rate of decline in groundwater level was -2.14 m per year (Fig. 3), with a significant negative trend ($p<0.01$, Sen's slope = -2.089) (Table 1). In the post-construction period (1997-2018), the rate of decline in groundwater level was reduced to -0.86 m per year (significant negative trend; p<0.0.05, Sen's slope = -0.669) (Table 2).

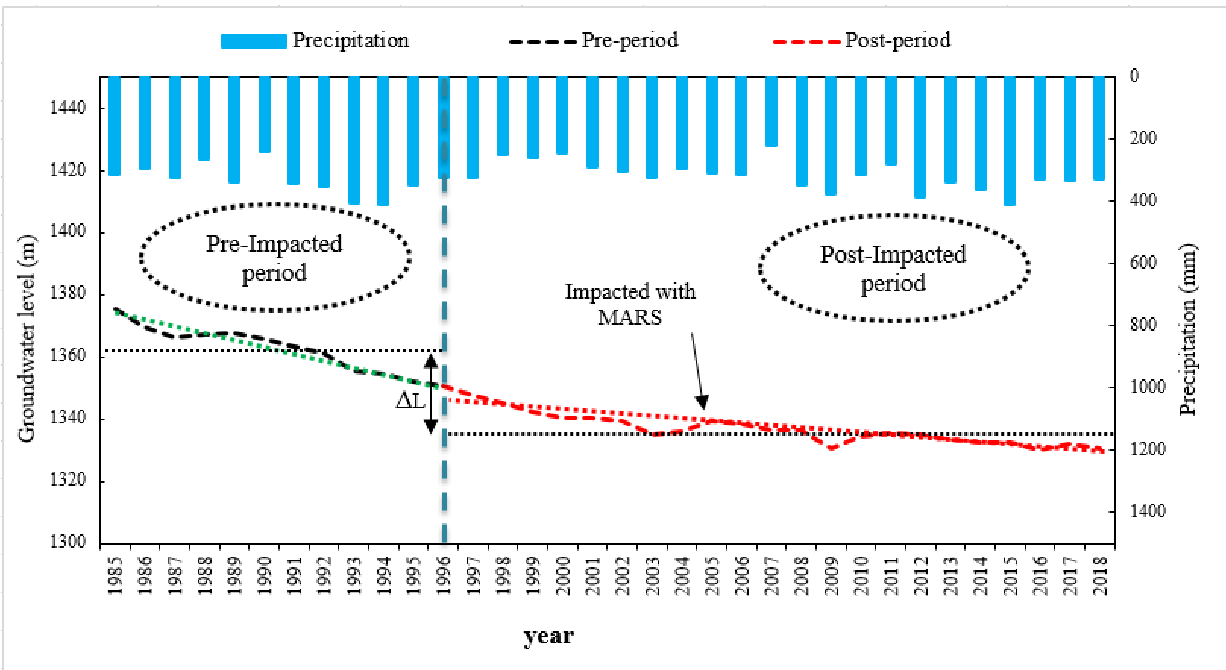

Fig. 3. Temporal variation in precipitation and groundwater level in the Shabestar aquifer in pre- and post-periods relative to managed aquifer recharge structure (MARS) construction.

Table 2. Results of the Mann-Kendall (MK) test and Sen's slope estimator (Sen) for precipitation and groundwater level in the Shabestar aquifer in periods pre- and post-construction of the managed aquifer recharge structure (MARS)

Parameter	Period	MK	p-value	Sen
Precipitation	1985-2018	1.200	0.229	0.956
Groundwater level	1985-2018	-4.561	0.045	-1.295
Groundwater level pre-period	1985-1996	-4.114	0.001	-2.089
Groundwater level post-period	1996-2018	-5.495	0.039	-0.669

3.2. Distribution of shear stress, velocity, and sedimentation in MARS ponds

There were clear signs of rotational flow in ponds #2 to #6, which led to sedimentation in these ponds (Fig. 4a). The modeling results showed two patterns of velocity distribution across the ponds: i) concentrated flow and high velocity near spillways and outlets (red color zone in Fig. 4a) and ii) lower velocity areas with increasing distance from the outlets (transition color from red to blue in Fig. 4a). This variation in flow velocity could result in differences in shear stress on the pond bed, leading to zoning with erosional and sedimentation areas (Fig. 4)

Due to the cascade configuration of the MARS layout, the flow velocity varied from 0.00 to 1.00 m/s within the ponds (Fig. 4a). The flow velocity also declined from upper ponds (#1-#4) to lower (#6, #7). The maximum flow velocity in ponds #6 and #7 was found to be below 0.3 m/s, and therefore the majority of transported particles entering these ponds could be expected to be deposited as sediment. Investigation of shear stress variations in MARS ponds showed the maximum shear stress in ponds #1 to #4, due to narrowing of the outlet and higher velocity (Fig. 4b), increasing the potential for erosion in these areas. In contrast, in downstream ponds (#6, #7) the shear stresses were low and sedimentation potential was high.

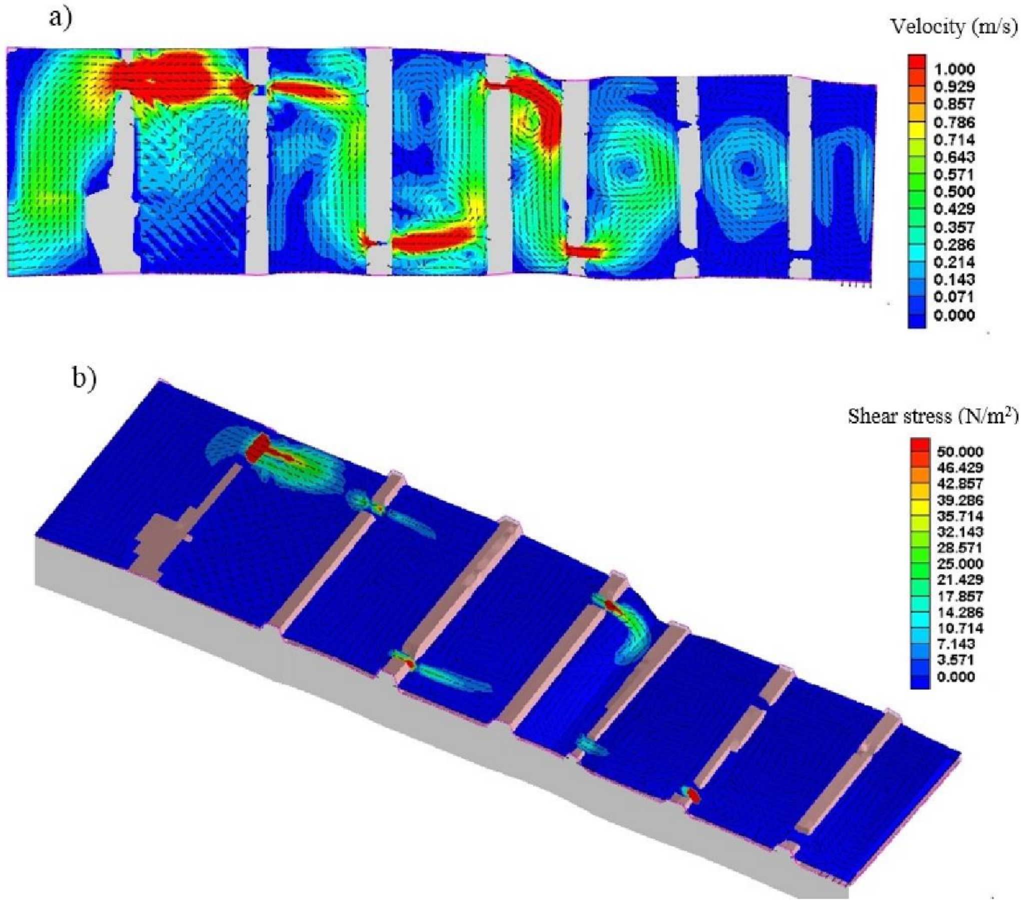

Fig. 4. a) Flow velocity and b) shear stress distribution along the series of ponds in Kaboutar-Ali Chay managed aquifer recharge structure (MARS).

In order to investigate sedimentation and erosion conditions in the MARS, long-term (14 days) and short-term (7 days) simulations were performed based on observed flow duration in the studied river reach. Evaluation of the changes in the bed of MARS ponds indicated that in many parts of the MARS (except for the outlet of the ponds), the decrease in cross-sectional area and increase in velocity resulted in a maximum depth of erosion of 0.65 and 0.77 m for short-term and long-term simulations at the inlet of pond #1 and outlet of pond #5, respectively (Fig. 5). The maximum height of sedimentation was 1.022 m in short-term (7 days) and 1.54 m in long-term (14 days) simulations (Fig. 5). The mean height of sedimentation was 0.57 and 0.60 m for short term and long-term periods, respectively. Also, the mean depth of erosion in the MARS ponds were 0.32 and 0.42 m for short term and long-term periods, respectively. Therefore, the ration of the erosion/sedimentation was achieved 0.57 and 0.70 for short term and long-term periods, respectively. This indicated that in for the long term the sedimentation processes in the MARSs have occurred more than the short-term. Therefore, in the long term, by trapping sediments in the ponds, flow discharge with the low amount of sediment released from the ponds and this flow to compensate for the lack of sediment and achieve transport capacity, not only does not sediment like the pattern of alluvial rivers but also causes erosion and consequently decreasing of the riverbed in the downstream. It is also worth mentioning that, due to sedimentation in the MARS ponds over time, the permeability of the pond bed material will decrease as the pores become clogged with sediment particles, decreasing the efficiency of the MARS in groundwater recharge.

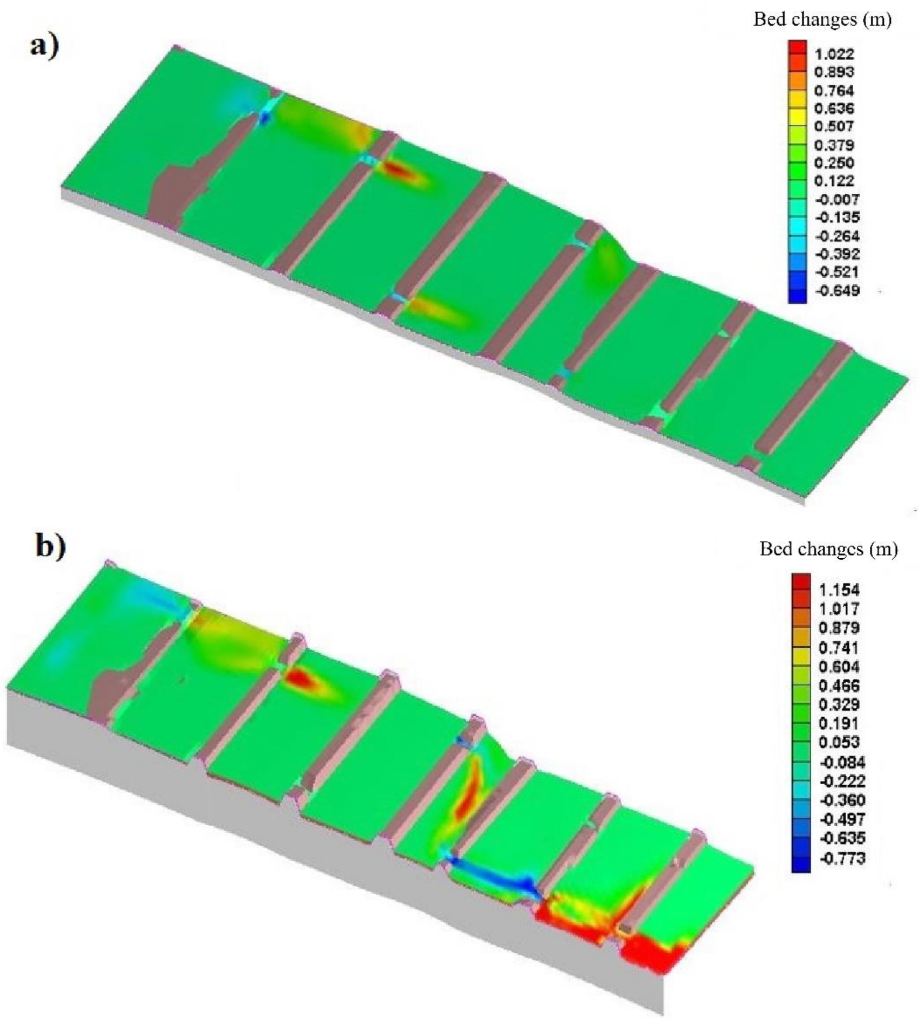

Fig. 5. Bed changes along the series of ponds in Kaboutar-Ali Chay managed aquifer recharge structure (MARS) in a) short-term (7-days) and b) long-term (14-days) simulations.

Based on the results obtained for velocity and shear stress distribution in the ponds, it can be concluded that the majority of transported particles from river headwaters, which play the main role in forming the alluvial fan, are now trapped in the MARS ponds. Thus, establishing the MARS at the top of Kaboutar-Ali-Chay alluvial fan (which plays a significant role in sediment transportation) has interrupted the sedimentation mechanism in the lower part of alluvial fan. In other words, the flow path and flow dynamics in the main body of the alluvial fan have been changed, with lower flow rate and sediment density at the outflow of the MARS, due to diversion of flood flow to the MARS ponds above the fan, so that very little sediment enters the alluvial fan. As a result, the sediment deposition process on the surface of the alluvial fan has become a sediment-erosion process. It is also worth mentioning that, due to sedimentation in the MARS ponds over time, the permeability of the pond bed material will decrease as the pores become clogged with sediment particles, decreasing the efficiency of the MARS in groundwater recharge.

Model validation, based on orthogonal assessment using ADO and MDO and smoothness assessment using AGAR and MGAR indices, indicated that the MARS mesh in the CCHE2D model was of high quality. This was based on ADO and MDO values of 2.21 and 2.28, respectively, where lower values indicate higher quality of the mesh, and AGAR and MGAR values of 1.06 and 1.10, where values closer to 1 indicate high quality of the mesh.

3.4. Assessment of morphological changes in the alluvial fan using remote sensing data

Morphological changes in the Kaboutar-Ali-Chay alluvial fan 1985-2018 are shown in Fig. 6 and Table 3). The main morphometric parameters, including area, perimeter, L_{AF}, R_f and S, showed decreasing rates over time (Table 3). The area of the alluvial fan decreased by 5.5 km^2 from 1985 to 2018, while the rate of decrease changed from -0.228 to -0.115 km^2/year from the period pre- to post- MARS construction. Similar decreases in the period 1985-2018 and a higher rate of change in pre-impact than post-impact periods were observed for other morphometric parameters, e.g., fan perimeter (rate change from -0.250

to -0.314 km/year for pre- and post- period, respectively), L_{AF} (rate change from -0.060 to -0.034 km/year for pre- and post-period, respectively), R_f (change from -0.009 to -0.006 for pre- and post- period, respectively), and S (change from -0.012% to 0.023% for pre- and post- period, respectively). The remaining parameters studied (S_{AF}, R_e, R_c, C_c) showed inconsistent increases and decreases in their rate of change in pre- and post- periods.

Table 3. Changes in morphometric parameters of the Kaboutar-Ali-Chay alluvial fan, 1984-2017

Year	Area	Perimeter	Length	Form factor	Shape factor	Elongation ratio	Circularity ratio	Compactness coefficient	Slope
	(km^2)	(km)	L_{AF}	R_f	S_{AF}	R_e	R_c	C_c	S
1984	12.84	34.62	5.592	1.148	2.436	0.723	0.140	2.726	6.742
1987	11.44	32.05	5.238	1.092	2.398	0.728	0.137	2.673	6.694
1990	10.92	31.69	5.102	1.071	2.383	0.731	0.135	2.705	6.641
1993	10.25	31.48	4.922	1.042	2.362	0.734	0.130	2.773	6.607
1996	9.87	31.36	4.816	1.025	2.350	0.736	0.126	2.816	6.588
1999	9.52	30.05	4.717	1.009	2.338	0.738	0.132	2.748	6.577
2002	9.03	26.81	4.579	0.986	2.322	0.740	0.158	2.517	6.551
2005	8.90	26.43	4.541	0.980	2.317	0.741	0.160	2.499	6.538
2008	8.63	26.00	4.462	0.967	2.308	0.743	0.160	2.497	6.507
2011	8.34	25.85	4.378	0.953	2.297	0.744	0.157	2.524	6.415
2014	7.90	25.68	4.244	0.931	2.280	0.747	0.151	2.578	6.306
2017	7.33	24.09	4.067	0.901	2.257	0.751	0.159	2.510	6.140

Table 4 presents the results of the paired samples t-test for the morphometric parameters during pre- and post-impact periods. As can be seen, all morphometric parameters (L_{AF}, R_f, S_{AF}, R_e, R_c, C_c, S) showed significant differences ($P<0.01$) between pre- and post-impact periods. It can be concluded that construction of MARS has had a significant impact on morphometric parameters in the Kaboutar-Ali-Chay alluvial fan.

By applying fundamental concepts of hydro-sediment dynamic modeling and feedback in the context of human-landscape systems, we demonstrated how morphological parameters in natural landscapes can be affected by anthropogenic activities. Specifically, the results revealed that restoration strategies in one part of water resources management (groundwater artificial recharge) can affect other parts of the environmental system (morphological changes in the Kaboutar-Ali-Chay alluvial fan). These results can be used by planners and decision-makers on IWRM to formulate appropriate actions.

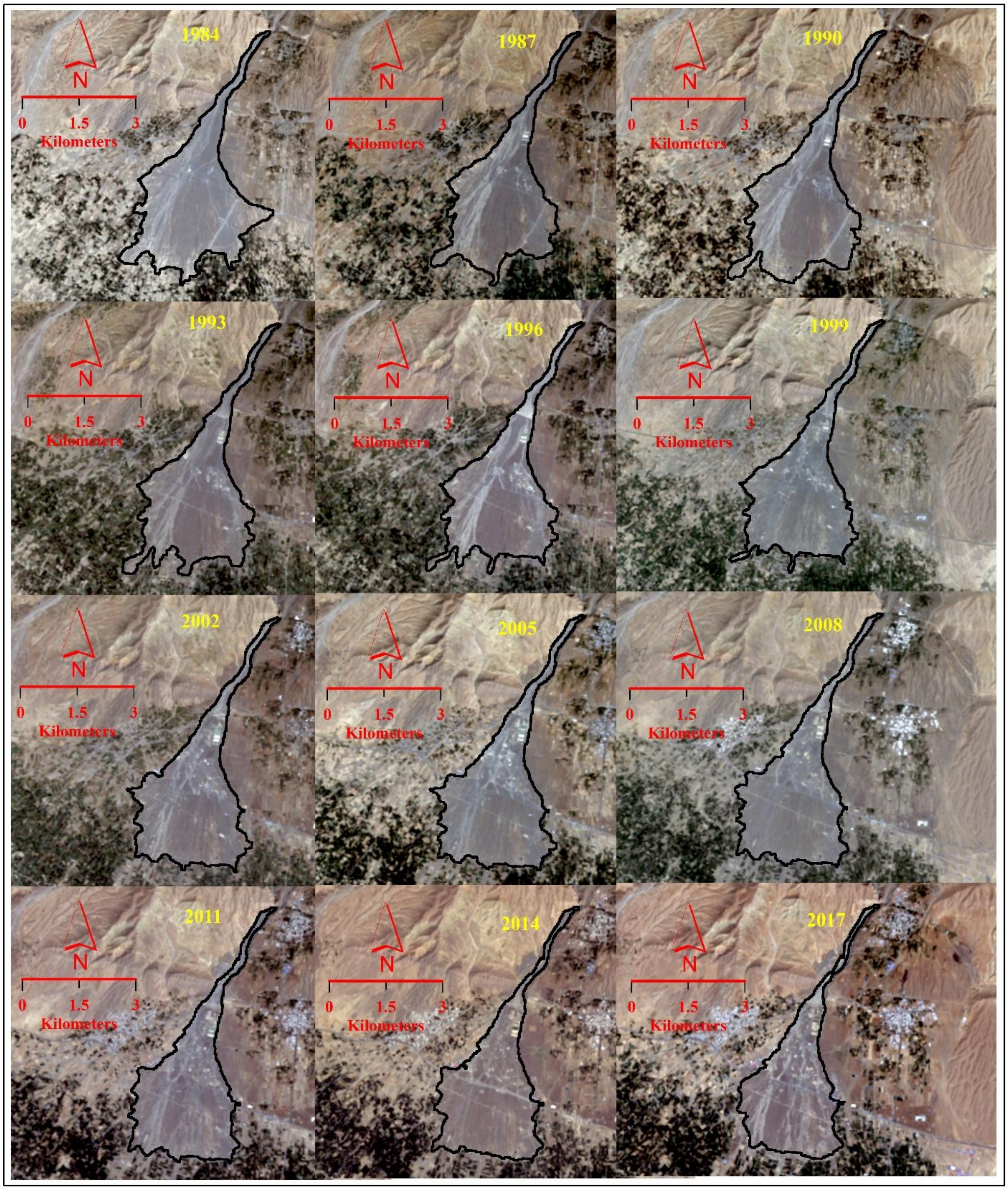

Fig. 6. Morphological changes in the Kaboutar-Ali-Chay alluvial fan between years in the period 1984-2017.

It is difficult to predict variations in human-impacted landscape systems (such as alluvial fans) because of the complexity of geomorphic and socio-environmental conditions. Previous studies have shown that changes in fluvial systems caused by anthropogenic influences are increasing over time (e.g., Comiti, 2012; Gumiero et al., 2015; Poeppl et al., 2017; Verstraeten et al., 2017). The extent of morphological change will be determined by the intensity of human impacts and by the sensitivity of the environment to natural disturbance. However, morphological changes in small areas reflect anthropogenic influences rather than environment sensitivity to natural disturbance.

Table 4. Results of paired samples t-test for alluvial fan area (A), perimeter (P) and the seven morphometric parameters tested (length of alluvial fan (L_{AF}), form factor (R_f), shape factor (S_{AF}), elongation ratio (R_e), circularity ratio (R_c), compactness coefficient (C_c), and slope (S)) during pre- and post-impact periods

	Paired Differences						
				95% Confidence Interval of the Difference			
Morphometric parameter	Mean	Std. Deviation	Std. Error Mean	Lower	Upper	t	Sig. (2-tailed)
A_{pre}-A_{post}	2.523	0.843	0.318	1.743	3.302	7.921	0.000
P_{pre}-P_{post}	5.745	1.008	0.381	4.813	6.678	15.083	0.000
L_{AFpre}-L_{AFpost}	0.703	0.233	0.088	0.487	0.918	7.973	0.000
R_{fpre}-R_{fpost}	0.114	0.038	0.014	0.079	0.149	7.985	0.000
S_{AFpre}-S_{AFpost}	0.083	0.028	0.011	0.057	0.109	7.835	0.000
Re_{pre}-Re_{post}	-0.013	0.004	0.002	-0.017	-0.009	-7.691	0.000
Rc_{pre}-Rc_{post}	-0.020	0.011	0.004	-0.031	-0.009	-4.617	0.004
Cc_{pre}-Cc_{post}	0.184	0.104	0.039	0.087	0.280	4.653	0.003
S_{pre}-S_{post}	0.219	0.150	0.057	0.080	0.358	3.869	0.008

4. Conclusions

In arid and semi-arid regions with limited available surface water, the groundwater resource is the most important and sometimes only source of water. Managed artificial recharge structures (MARS) are commonly re-used to recharge this vital resource, by diverting and storing surface water (particularly floodwater) in ponds for re-infiltration into the aquifer. MARS has considerable advantages, but also a major disadvantage through its influence on the natural fluvial system. This study quantified the impact of the Kaboutar-Ali-Chay MARS in Northwestern Iran on groundwater recharge, using observed data from groundwater wells, and on the downstream alluvial fan, by combining the results of hydro-sediment modeling with remote sensing data. The results revealed that sedimentation in MARS ponds had led to changes in the alluvial fan. The results for groundwater levels revealed a significant negative trend despite increasing precipitation rate in the study period (1985-2018), but the MARS system decreased the rate of groundwater decline from -2.14 m/year (1985-1996, before MARS construction) to -0.86 m/year (1997-2018, after MARS construction). Modeling results for the seven ponds in Kaboutar-Ali-Chay MARS showed decreases in flow velocity (1.0-0.0 m/s) and shear stress (50-0.0 N/m^2) from upstream to downstream ponds, with accompanying increases in sedimentation compared with the unregulated flood flow system. Remote sensing analysis revealed decreases in area and significant ($p<0.01$) changes in different morphometric parameters of the alluvial fan (L_{AF}, R_f, S_{AF}, R_e, R_c, C_c, S) between the periods pre- and post- MARS construction.

References

1. Abou Zaki, N., Torabi Haghighi, A., M Rossi, P., J Tourian, M., & Kløve, B. (2019). Monitoring Groundwater Storage Depletion Using Gravity Recovery and Climate Experiment (GRACE) Data in Bakhtegan Catchment, Iran. *Water*, *11*(7), 1456.
2. Ameri, A. A., Pourghasemi, H. R., & Cerda, A. (2018). Erodibility prioritization of sub-watersheds using morphometric parameters analysis and its mapping: A comparison among TOPSIS, VIKOR, SAW, and CF multi-criteria decision-making models. *Science of the Total Environment*, *613*, 1385-1400.
3. Bari, S. H., Rahman, M. T. U., Hoque, M. A., & Hussain, M. M. (2016). Analysis of seasonal and annual rainfall trends in the northern region of Bangladesh. *Atmospheric Research*, *176*, 148-158.
4. Beigi, E., & Tsai, F. T. C. (2015). Comparative study of climate-change scenarios on groundwater recharge, southwestern Mississippi and southeastern Louisiana, USA. *Hydrogeology Journal*, *23*(4), 789-806.

5. Cai, Z., & Ofterdinger, U. (2016). Analysis of groundwater-level response to rainfall and estimation of annual recharge in fractured hard rock aquifers, NW Ireland. *Journal of Hydrology*, *535*, 71-84.
6. Cao, G., Scanlon, B. R., Han, D., & Zheng, C. (2016). Impacts of thickening unsaturated zone on groundwater recharge in the North China Plain. *Journal of hydrology*, *537*, 260-270.
7. Carrera-Hernández, J. J., Smerdon, B. D., & Mendoza, C. A. (2012). Estimating groundwater recharge through unsaturated flow modelling: Sensitivity to boundary conditions and vertical discretization. *Journal of Hydrology*, *452*, 90-101.
8. Chang, I. S., Zhao, M., Chen, Y., Guo, X., Zhu, Y., Wu, J., & Yuan, T. (2020). Evaluation on the integrated water resources management in China's major cities-Based on City Blueprint® Approach. *Journal of Cleaner Production*, 121410.
9. Chenini, I., Mammou, A. B., & El May, M. (2010). Groundwater recharge zone mapping using GIS-based multi-criteria analysis: a case study in Central Tunisia (Maknassy Basin). *Water Resources Management*, *24*(5), 921-939.
10. Chenini, I., Msaddek, M. H., & Dlala, M. (2019). Hydrogeological characterization and aquifer recharge mapping for groundwater resources management using multicriteria analysis and numerical modeling: A case study from Tunisia. *Journal of African Earth Sciences*, *154*, 59-69.
11. Comiti, F. (2012). How natural are Alpine Mountain Rivers? Evidence from the Italian Alps. *Earth Surface Processes and Landforms*, *37*(7), 693-707.
12. Giardino, C., Brando, V. E., Dekker, A. G., Strömbeck, N., & Candiani, G. (2007). Assessment of water quality in Lake Garda (Italy) using Hyperion. *Remote Sensing of Environment*, *109*(2), 183-195.
13. Gumiero, B., Rinaldi, M., Belletti, B., Lenzi, D., & Puppi, G. (2015). Riparian vegetation as indicator of channel adjustments and environmental conditions: the case of the Panaro River (Northern Italy). *Aquatic sciences*, *77*(4), 563-582.
14. Haghighi, A. T., Darabi, H., Shahedi, K., Solaimani, K., & Kløve, B. (2020). A scenario-based approach for assessing the hydrological impacts of land use and climate change in the Marboreh Watershed, Iran. *Environmental Modeling & Assessment*, *25*(1), 41-57.
15. Haghighi, A. T., Fazel, N., Hekmatzadeh, A. A., & Klöve, B. (2018). Analysis of effective environmental flow release strategies for Lake Urmia restoration. *Water Resources Management*, *32*(11), 3595-3609.
16. Haghighi, A. T., Marttila, H., & Kløve, B. (2014). Development of a new index to assess river regime impacts after dam construction. *Global and Planetary Change*, *122*, 186-196.

17. Hartmann, H., Snow, J. A., Su, B., & Jiang, T. (2016). Seasonal predictions of precipitation in the Aksu-Tarim River basin for improved water resources management. *Global and Planetary Change*, *147*, 86-96.
18. Huang, T., Ma, B., Pang, Z., Li, Z., Li, Z., & Long, Y. (2019). How does precipitation recharge groundwater in loess aquifers? Evidence from multiple environmental tracers. *Journal of Hydrology*, 124532.
19. Huang, T., Pang, Z., & Yuan, L. (2013). Nitrate in groundwater and the unsaturated zone in (semi) arid northern China: baseline and factors controlling its transport and fate. *Environmental earth sciences*, *70*(1), 145-156.
20. Jia, Y., & Wang, S. S. (1999). Numerical model for channel flow and morphological change studies. *Journal of Hydraulic Engineering*, *125*(9), 924-933.
21. Kalbus, E., Reinstorf, F., & Schirmer, M. (2006). Measuring methods for groundwater? Surface water interactions: a review. *Hydrology and Earth System Sciences Discussions*, *10*(6), 873-887.
22. Kamanbedast, A. A., Akib, S., & Khadem, K. (2018). Investigation of Epi structure in frontal of intakes on diversion flow in river bend with cche2d model. *Fresen Environ bulletin*, *27(2):* 807–814.
23. Koller, M., Sandholzer, D., Salerno, A., Braunegg, G., & Narodoslawsky, M. (2013). Biopolymer from industrial residues: Life cycle assessment of poly (hydroxyalkanoates) from whey. *Resources, conservation and recycling*, *73*, 64-71.
24. Kroes, J., van Dam, J., Supit, I., De Abelleyra, D., Verón, S., de Wit, A., & Wesseling, J. (2019). Agrohydrological analysis of groundwater recharge and land use changes in the Pampas of Argentina. *Agricultural water management*, *213*, 843-857.
25. Lin, R., & Wei, K. (2006). Tritium profiles of pore water in the Chinese loess unsaturated zone: implications for estimation of groundwater recharge. *Journal of Hydrology*, *328*(1-2), 192-199.
26. Liu, J., Qin, K., Zhen, L., Xiao, Y., & Xie, G. (2019). How to allocate interbasin water resources? A method based on water flow in water-deficient areas. *Environmental Development*, 100460.
27. Liu, W., Zhang, X. C., Dang, T., Ouyang, Z., Li, Z., Wang, J., & Gao, C. (2010). Soil water dynamics and deep soil recharge in a record wet year in the southern Loess Plateau of China. *Agricultural Water Management*, *97*(8), 1133-1138.
28. Lu, H., Bryant, R. B., Buda, A. R., Collick, A. S., Folmar, G. J., & Kleinman, P. J. (2015). Long-term trends in climate and hydrology in an agricultural, headwater watershed of central Pennsylvania, USA. *Journal of Hydrology: Regional Studies*, *4*, 713-731.

29. Lu, W. X., Zhao, Y., Chu, H. B., & Yang, L. L. (2014). The analysis of groundwater levels influenced by dual factors in western Jilin Province by using time series analysis method. *Applied Water Science*, *4*(3), 251-260.
30. Mohammadzadeh, H., & Heydarizad, M. (2020). A conceptual model for water resources circulation patterns in Andarokh-Kardeh region (NE, Iran). *Geochemistry*, 125593.
31. Moussa, A. M. A. (2010). Solving the problem of sedimentation at water intake of Rowd El-Farag pump station using 2D model. *Ain Shams Engineering Journal*, *1*(2), 103-114.
32. Nassar, M. A. (2011). Multi-parametric sensitivity analysis of CCHE2D for channel flow simulations in Nile River. *Journal of hydro-environment research*, *5*(3), 187-195.
33. OhIsson, L. (2000). Water conflicts and social resource scarcity. *Physics and Chemistry of the Earth, Part B: Hydrology, Oceans and Atmosphere*, *25*(3), 213-220.
34. Poeppl, R. E., Keesstra, S. D., & Maroulis, J. (2017). A conceptual connectivity framework for understanding geomorphic change in human-impacted fluvial systems. *Geomorphology*, *277*, 237-250.
35. Poongodi, R., & Venkateswaran, S. (2018). Prioritization of the micro-watersheds through morphometric analysis in the Vasishta Sub Basin of the Vellar River, Tamil Nadu using ASTER Digital Elevation Model (DEM) data. *Data in brief*, *20*, 1353-1359.
36. Rad, P. H., Kamanbedast, A., Heidarnejad, M., Masjedi, A., & Hasonizadeh, H. (2019). The effect of convergence and divergence on flow pattern and sediment transport in lateral intakes using physical and numerical models. *Ain Shams Engineering Journal*. In Press.
37. Rezaei, A., Zare, M., Raeisi, E., & Ghanbari, R. N. (2013). Interaction of a fresh water lake and a karstic spring via a syncline fold. *Groundwater*, *51*(2), 305-312.
38. Safavi, H. R., Mehrparvar, M., & Szidarovszky, F. (2016). Conjunctive management of surface and ground water resources using conflict resolution approach. *Journal of Irrigation and Drainage Engineering*, *142*(4), 05016001.
39. Sang, Y. F., Wang, Z., & Liu, C. (2014). Comparison of the MK test and EMD method for trend identification in hydrological time series. *Journal of Hydrology*, *510*, 293-298.
40. Shahrood, A. J., Menberu, M. W., Darabi, H., Rahmati, O., Rossi, P. M., Kløve, B., & Haghighi, A. T. (2020). RiMARS: An automated river morphodynamics analysis method based on remote sensing multispectral datasets. *Science of The Total Environment*, *719*, 137336.
41. Sindhu, D., Ravikumar, A. S., & Shivakumar, B. L. (2015). Quantitative Analysis of Catchment using remote sensing and Geographic Information system. *Aquatic Procedia*, *4*, 1421-1428.

42. Sohn, W., Jeong, M., & Jeong, K. (2020). Theoretical comparative study of t tests and nonparametric tests for final status surveys of MARSSIM at decommissioning sites. *Annals of Nuclear Energy*, *135*, 106945.
43. Tan, H., Liu, Z., Rao, W., Jin, B., & Zhang, Y. (2017). Understanding recharge in soil-groundwater systems in high loess hills on the Loess Plateau using isotopic data. *Catena*, *156*, 18-29.
44. Torabi Haghighi, A., Abou Zaki, N., Rossi, P. M., Noori, R., Hekmatzadeh, A. A., Saremi, H., & Kløve, B. (2020). Unsustainability Syndrome—From Meteorological to Agricultural Drought in Arid and Semi-Arid Regions. *Water*, *12*(3), 838.
45. Torabi Haghighi, A., Sadegh, M., Behrooz-Koohenjani, S., Hekmatzadeh, A. A., Karimi, A., & Kløve, B. (2020). The mirage water concept and an index-based approach to quantify causes of hydrological changes in semi-arid regions. *Hydrological Sciences Journal*, *65*(2), 311-324.
46. Verstraeten, G., Broothaerts, N., Van Loo, M., Notebaert, B., D'Haen, K., Dusar, B., & De Brue, H. (2017). Variability in fluvial geomorphic response to anthropogenic disturbance. *Geomorphology*, *294*, 20-39.
47. Volpe, V., Silvestri, S., & Marani, M. (2011). Remote sensing retrieval of suspended sediment concentration in shallow waters. *Remote Sensing of Environment*, *115*(1), 44-54.
48. Yadav, M., & Setia, B. (2016). Conceptualization and Design of an Efficient Groundwater Recharge system for NIT Kurukshetra. *Procedia Technology*, *25*, 138-145.
49. Yang, Z., Song, J., Cheng, D., Xia, J., Li, Q., & Ahamad, M. I. (2019). Comprehensive evaluation and scenario simulation for the water resources carrying capacity in Xi'an city, China. *Journal of environmental management*, *230*, 221-233.
50. Yaraghi, N., Ronkanen, A. K., Darabi, H., Kløve, B., & Haghighi, A. T. (2019). Impact of managed aquifer recharge structure on river flow regimes in arid and semi-arid climates. *Science of the Total Environment*, *675*, 429-438.
51. Yasuda, H., Berndtsson, R., Hinokidani, O., Huang, J., Saito, T., Zheng, J., & Kimura, R. (2012). The impact of plant water uptake and recharge on groundwater level at a site in the Loess Plateau of China. *Hydrology Research*, *44*(1), 106-116.
52. Yawson, D. O., Adu, M. O., Mulholland, B., Ball, T., Frimpong, K. A., Mohan, S., & White, P. J. (2019). Regional variations in potential groundwater recharge from spring barley crop fields in the UK under projected climate change. *Groundwater for Sustainable Development*, *8*, 332-345.

53. Zaki, N. A., Haghighi, A. T., Rossi, P. M., Tourian, M. J., & Kløve, B. (2018). Monitoring groundwater storage depletion using gravity recovery and climate experiment (GRACE) data in the semi-arid catchments.

54. Zhang, J., Chen, Y., Li, Z., Song, J., Fang, G., Li, Y., & Zhang, Q. (2019). Study on the utilization efficiency of land and water resources in the Aral Sea Basin, Central Asia. *Sustainable Cities and Society*, *51*, 101693.

55. Zhang, Y. Q., Wang, J. H., Chen, J. J., & Li, M. G. (2017). Numerical study on the responses of groundwater and strata to pumping and recharge in a deep confined aquifer. *Journal of Hydrology*, *548*, 342-352.

56. Zhang, Y., & Jia, Y. (2005). CCHE2D Mesh Generator Users' Manual—Version 2.50. *National Center for Computational Hydrosicence and Engineering*, *Technical Report: NCCHE-TR-2005-05*.

57. Zhang, Y., & Jia, Y. (2013). Parallelized CCHE2D flow model with CUDA Fortran on Graphics Processing Units. *Computers & Fluids*, *84*, 359-368.